Available online at www.sciencedirect.com

ScienceDirect

Mendeleev Commun., 2024, **34**, 601–603

Mendeleev Communications

Effect of particle size of titanium oxide β-Ti_3O_5 on its thermal stability

Albina A. Valeeva,*[a] Evgeny Yu. Gerasimov[b] and Olga G. Reznitskikh[a]

[a] *Institute of Solid State Chemistry, Ural Branch of the Russian Academy of Sciences, 620990 Ekaterinburg, Russian Federation. Fax: +7 343 374 4495; e-mail: anibla_v@mail.ru*

[b] *G. K. Boreskov Institute of Catalysis, Siberian Branch of the Russian Academy of Sciences, 630090 Novosibirsk, Russian Federation*

DOI: 10.1016/j.mencom.2024.06.043

It was established that the particle size of titanium oxide β-Ti_3O_5 has a great influence on the processes of phase formation and the stability of particles during heating. It was shown that at a temperature of about 456 K, β-Ti_3O_5 microcrystals undergo a reversible first-order phase transition, in which the low-temperature β-Ti_3O_5 phase is transformed into the high-temperature λ-Ti_3O_5 phase, and at higher temperatures the β-Ti_3O_5 phase is partially oxidized to form the Magnéli phase Ti_4O_7. It was found that β-Ti_3O_5 nanocrystals are unstable in an argon atmosphere and at temperatures above 400 K the β-Ti_3O_5 powder is oxidized.

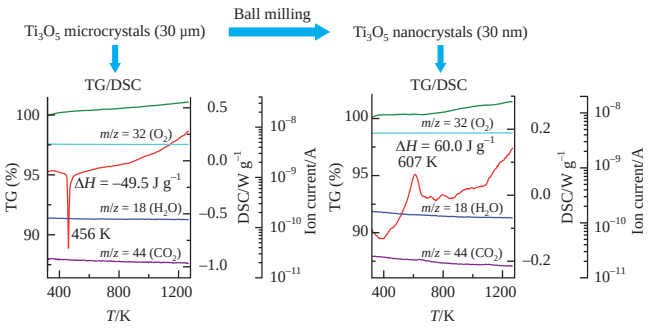

Keywords: titanium oxide, Ti_3O_5, nanocrystal, XRD, SEM, TEM, TG, DSC.

The production of functional nanomaterials with developed surfaces and controlled properties is an important part of rapidly evolving technologies. There are more and more works devoted to the search for materials whose structure and properties are governed by nonstoichiometry, particle size and changes in morphology, crystal structure or both, as well as their production methods.[1–5] Titanium oxides are effective materials in various fields due to the diversity of their functional properties, which reflect the variety of its modifications, crystal structures, physical properties, morphologies and particle sizes.[6–10] These compounds are in demand and are widely used in the development of promising functional materials for efficient photoelectric transducers, memristor memory cells, renewable energy sources, photocatalysis, adsorption, coating and others.[11–14] The Ti–O system contains titanium oxide Ti_3O_5, which under certain conditions undergoes a semiconductor–metal phase transition. In addition, there is an abrupt change in electrical, magnetic and structural characteristics, which is very attractive for use in microelectronics.[15–21] The stability of microcrystalline titanium oxide Ti_3O_5 was first studied by Rusakov,[22] who discovered a phase transition at a temperature of about 448 K. In the case of microcrystalline Ti_3O_5 oxide, available literature data on the temperature of the phase transition from the low-temperature semiconductor β-Ti_3O_5 phase, stable at room temperature, to the metastable high-temperature metallic β-Ti_3O_5 phase vary and are scattered over a rather wide temperature range from 373 to 463 K.[15–24] Besides, a first-order phase transition from the α-Ti_3O_5 phase to the β-Ti_3O_5 phase was noted at 460 K during heating and at 440 K during cooling.[18] The metallic α-Ti_3O_5 phase is stable at higher temperatures and crystallizes in an orthorhombic structure (space group *Cmcm*),[18] while the semiconductor phase (β-Ti_3O_5) has a stable monoclinic structure (space group *C*2/*m*) at room temperature. Other phase transitions between the monoclinic γ-Ti_3O_5 polymorph (space group *I*2/*c*) and the monoclinic δ-Ti_3O_5 phase (space group *P*2/*a*) were also determined.[24] The study on nanosized λ-Ti_3O_5 demonstrated that the metastable λ-Ti_3O_5 phase with a monoclinic structure (space group *C*2/*m*) cannot exist in a macrocrystalline state and is stable only due to nanoscale effects.[18] In this regard, the preparation of Ti_3O_5 nanopowder and the study of phase transitions in titanium oxide Ti_3O_5 depending on the particle size is an urgent task. The purpose of this work was to synthesize titanium oxide Ti_3O_5 nanoparticles by high-energy milling and study the stability of the powder at high temperatures.[†]

The XRD pattern (Figure 1) of synthesized Ti_3O_5 exhibits reflections corresponding to the low-temperature β-Ti_3O_5 phase

[†] The initial β-Ti_3O_5 microcrystals with an average size of ~30 μm were synthesized by solid-phase vacuum sintering of a mixture of Ti and TiO_2 powders at a temperature of 1773 K in a vacuum of 10^{-3} Pa. The crushing of the initial microcrystalline powders was performed by high-energy milling in a Retsch PM200 planetary mill using beakers (125 ml) and grinding balls (d = 3 mm) made of zirconium dioxide ZrO_2 stabilized with yttria Y_2O_3. The experiment was carried out under the following conditions: milling in isopropyl alcohol, balls-to-powder mass ratio of 10 : 1, rotation velocity of the backing plate 500 rpm, milling duration of 15, 30, 60, 120, 240 and 480 min with a change of direction every 15 min and a pause of 5 s.

X-ray diffraction (XRD) patterns of the powders were obtained on a Shimadzu XRD-7000 automatic diffractometer in the Bragg–Brentano geometry using CuK$\alpha_{1,2}$ radiation in the 2θ angle range from 10 to 150° with a scanning step of $\Delta(2\theta)$ = 0.02°. The ICDD powder diffraction database (USA, Release 2016) was used for phase identification. X-ray phase analysis was carried out using the Powder Cell 2.4 program. The dimensional and deformation contributions to the broadening of reflections were determined by the Williamson–Hall method.[25,26] To analyze the specific surface area and pore distribution on the surface of the samples, a Micromeritics Gemini VII 2390 analyzer was used, implementing the Brunauer–Emmett–Teller method with preliminary degassing at 393 K.

The morphology and structure of the powders were studied by scanning electron microscopy (SEM) on a Hitachi Regulus SU 8230 FE-SEM microscope with an accelerating voltage of 2 kV. The crystal structure and microstructure of the samples were also studied by transmission electron

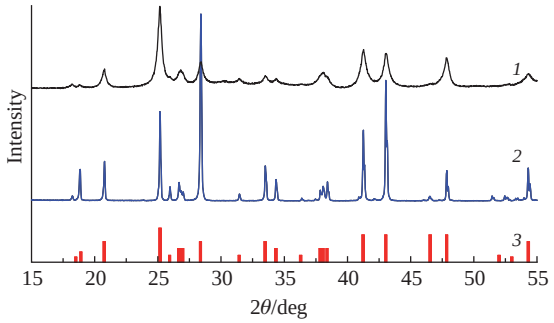

Figure 1 XRD patterns of (*1*) Ti_3O_5 nanocrystals and (*2*) Ti_3O_5 microcrystals. Additionally, the XRD pattern of (*3*) the JCPDF card (PDF no. 00-011-0217) is given as a reference for identifying the Ti_3O_5 phase.

with a monoclinic structure (space group *C*2/*m*, PDF no. 00-011-0217). The synthesized powder is single-phase and homogeneous, and splitting of reflections is observed. Figure 1 also shows the XRD pattern of β-Ti_3O_5 nanopowder produced by high-energy milling in a planetary mill for 480 min. According to XRD analysis, the crystal structure of β-Ti_3O_5 (space group *C*2/*m*) is stable, that is, high-energy milling does not lead to any phase transitions. The structure of β-Ti_3O_5 remains monoclinic, in contrast to titanium monoxide, in which the degree of long-range order decreases,[27] and from anatase, the milling of which leads to the formation of high-pressure phases.[28,29] The XRD patterns of milled β-Ti_3O_5 show a broadening of reflections associated with the small particle size and microdeformations. The dimensional and deformation contributions to the broadening of reflections were determined by the Williamson–Hall method. The calculations showed that as a result of milling, the coherent scattering region decreases from 30 μm to approximately 30 nm, and microdeformations increase from 0.02% for the initial powder to 0.49% for the milled powder. Analysis of nitrogen adsorption isotherms (77 K) made it possible to estimate the specific surface area of the initial and ground powder, which is equal to 0.122 ± 0.005 and 17.194 ± 0.348 $m^2\ g^{-1}$, respectively.

The morphology and crystal structure of the initial and milled powder were studied by SEM and TEM. In SEM images (Figure 2) of microcrystalline powder, well-faceted Ti_3O_5 particles several tens of microns in size are observed. As a rule, the particles have the shape of polyhedrons and are randomly oriented [Figure 2(*a*)]. At higher magnifications, it is seen that the developed facets have their own structure, consisting of cube-shaped crystals like rock salt [Figure 2(*b*)]. Figure 3 shows SEM micrographs of the milled Ti_3O_5 powder. The sample consists of rounded agglomerates of particles ~1 μm in size [Figure 3(*a*)]. The agglomerates are formed from individual crystallites ~100 nm in size. Besides, smaller particles in the size range of 5–50 nm randomly cover the surface of the crystallites [Figure 3(*b*)].

According to TEM data, the Ti_3O_5 nanopowder consists of lamellar particles ranging in size from 20 nm to 1 μm [Figure 4(*a*)].

microscopy (TEM) using a JEOL JEM 2010 transmission electron microscope with an accelerating voltage of 200 kV and a limiting resolution of 0.14 nm. EDX analysis was performed using a Bruker XFlash detector with a resolution of 128 eV.

Analyses by thermogravimetry (TG) and differential scanning calorimetry (DSC) were performed on a Netzsch STA 449 F3 Jupiter thermal analyzer using a thin-walled dish-shaped platinum crucible with the same initial sample weight of ~15 mg. Heating was carried out from 298 to 1273 K at a rate of 10 K min^{-1} in an argon atmosphere. The gas supply rate was 20 ml min^{-1}. The effluent gases were analyzed on a Netzsch QMS 403 Aëolos Quadro Jupiter quadrupole mass spectrometer, capillary-integrated with the thermal analyzer. High-purity argon was used in the work without additional purification from impurities (volume fractions of argon 99.998%, nitrogen ⩽ 0.0008%, oxygen ⩽ 0.0002%, water vapor ⩽ 0.0009%, carbon compounds in terms of CO_2 ⩽ 0.0001%).

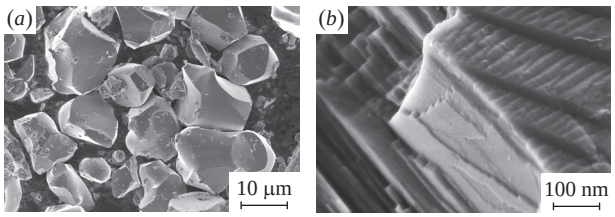

Figure 2 SEM images of Ti_3O_5 microcrystals: (*a*) polyhedron-shaped particles and (*b*) developed facets consisting of cubic rock-salt-type crystals.

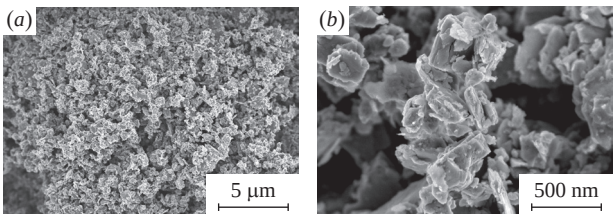

Figure 3 SEM images of Ti_3O_5 nanocrystals. (*a*) Nanocrystals stick to each other and form agglomerates. (*b*) Particles in the 5–50 nm size range cover the surface of the crystallites.

The particles are disordered, and extinction lines are observed on larger crystallites, which correspond to rather large microstresses in the crystal structure. According to the structure of the blocks, the sample can be divided into two parts. The first part has a well-crystallized structure, in which the block size reaches 100 nm. The second part is a less ordered structure, where, in addition to crystallites about 10 nm in size, areas of strong disorder (amorphization) are visible. Based on the observed interplanar spacing [Figure 4(*b*)], the powder can be attributed to the Ti_3O_5 structure (PDF no. 00-011-0217). EDX analysis data of a wide area show that, in addition to Ti, the sample contains Zr (1 wt%) impurities, which entered the system during high-energy milling from the grinding balls and beaker.

Using DSC, the effect of particle size on the thermal stability of Ti_3O_5 was studied and possible phase transitions occurring in titanium oxides Ti_3O_5 in the temperature range from 298 to 1273 K in an argon atmosphere were simultaneously investigated. Thermograms of microcrystals and nanocrystals of Ti_3O_5 are presented in Figures 5(*a*) and 5(*b*), respectively. The DSC curve of microcrystalline titanium oxide exhibits an endothermic peak (ΔH = −49.5 J g^{-1}) with an onset temperature (T_{onset}) of 456 K, which is related to a first-order phase transition from the low-temperature β-Ti_3O_5 phase to the high-temperature λ-Ti_3O_5 phase.[15,16] Throughout the experiment, the weight of the sample increased, which is associated with partial oxidation of Ti_3O_5. According to XRD data, after measurements by DSC, the powder consisted of a mixture of Ti_3O_5 (~82 wt%) and Ti_4O_7 (~18 wt%) phases. The overall weight gain was 0.6%. The phase transition at ~456 K was studied in detail. For this purpose, the temperatures of the beginning (456 K), middle (468 K) and end (503 K) of the phase transition were chosen. Below these temperatures, thermo-

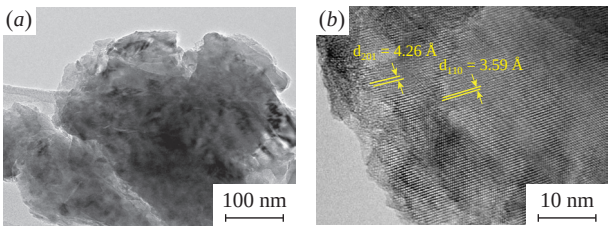

Figure 4 TEM images of Ti_3O_5 nanocrystals. (*a*) The powder consists of lamellar particles ranging in size from 20 nm to 1 μm. (*b*) Interplanar spacing corresponds to the Ti_3O_5 phase.

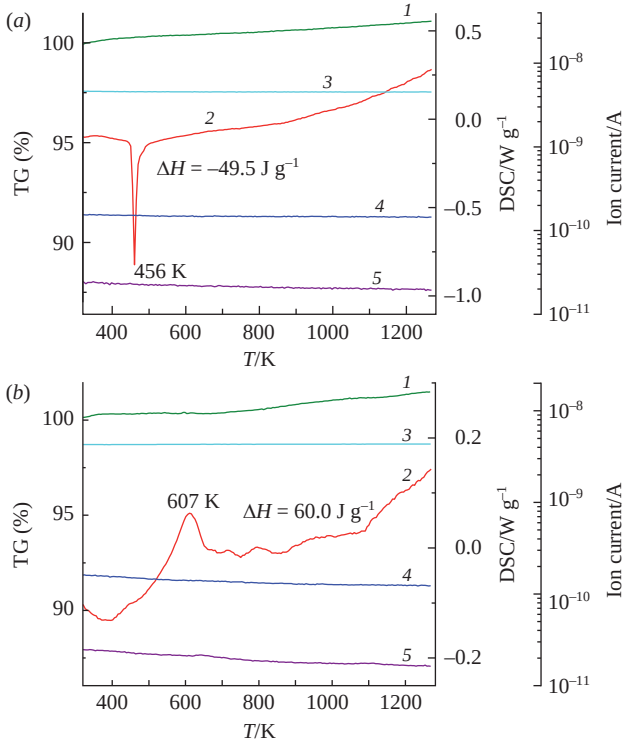

Figure 5 (*1*) TG and (*2*) DSC curves of Ti_3O_5. (*a*) For microcrystals, a sharp reversible endothermic peak (ΔH = −49.5 J g^{-1}) is observed at 456 K. (*b*) For nanocrystals, an exothermic peak at 607 K (ΔH = 60 J g^{-1}) is accompanied by the release of carbon dioxide. Mass spectrometry data are presented as the dependence of ion current values on temperature for gases (*3*) O_2 (*m*/*z* 32), (*4*) H_2O (*m*/*z* 18) and (*5*) CO_2 (*m*/*z* 44).

grams were taken under the same conditions as in the first experiment. After reaching the selected temperature, heating was stopped, the sample was cooled and examined by XRD analysis. Analysis of XRD patterns showed that in all the cases a reversible first-order phase transition occurs, in which the low-temperature β-Ti_3O_5 phase transforms into the high-temperature λ-Ti_3O_5 phase. Both of these phases belong to the monoclinic crystal system (space group *C*2/*m*). This transition is reversible, therefore, only the low-temperature β-Ti_3O_5 phase is recorded in the XRD patterns after DSC analysis.

When heating nanocrystalline Ti_3O_5, an exothermic thermal effect is observed in the temperature range from 470 to 670 K with a maximum at 607 K (ΔH = 60 J g^{-1}), which is most likely associated with desorption from the surface of the nanopowder of isopropyl alcohol used as a liquid medium for grinding Ti_3O_5 microcrystals.[30] This exothermic peak is accompanied by the release of carbon dioxide (*m*/*z* = 44), which is detected by a mass spectrometer. According to TG data, the weight of the sample increased by 1.2%. According to XRD data, after DSC measurements in an argon atmosphere, the powder of nanocrystalline titanium oxide Ti_3O_5 was oxidized and consisted of a mixture of phases Ti_4O_7 (47 wt%), Ti_5O_9 (19 wt%), Ti_6O_{14} (19 wt%), Ti_9O_{17} (7 wt%), rutile TiO_2 (7 wt%) and ZrO_2 (1 wt%). It is possible that even a small concentration of oxygen contained in argon causes oxidation of titanium oxide. Thus, experimental data suggest thermal instability of titanium oxide Ti_3O_5 in an argon atmosphere above 400 K.

In this work, we studied the influence of the particle size of the β-Ti_3O_5 phase with a monoclinic structure (space group *C*2/*m*) on its stability during milling in a planetary mill and in a DSC experiment when heated in the temperature range of 298–1273 K in an argon atmosphere. It has been established that particle size has a great influence on the processes of phase formation and the stability of particles during heating The DSC curve of microcrystalline titanium oxide Ti_3O_5 exhibits an endothermic peak (ΔH = −49.5 J g^{-1}) with an onset temperature of 456 K, which is related to a first-order phase transition from the low-temperature β-Ti_3O_5 phase to the high-temperature λ-Ti_3O_5 phase. At higher temperatures, Ti_3O_5 is partially oxidized. Nanocrystalline titanium oxide β-Ti_3O_5 is also unstable in an argon atmosphere and at temperatures above 400 K the nanopowder is oxidized.

This work was carried out within the framework of the state assignment for the Institute of Solid State Chemistry of the Ural Branch of the Russian Academy of Sciences (project no. MON RF FUWF-2024-0010). Electron microscopic experiments were performed using the equipment of the shared research center 'National Center of Investigation of Catalysts' at the Boreskov Institute of Catalysis.

References

1 E. P. Estévez Ruiz, J. López Lago and S. P. Thirumuruganandham, *Materials*, 2023, **16**, 3076.
2 O. V. Almjasheva, N. A. Lomanova, V. I. Popkov, O. V. Proskurina, E. A. Tugova and V. V. Gusarov, *Nanosyst.: Phys., Chem., Math.*, 2019, **10**, 428.
3 D. Chen, C. Chen, Z. M. Baiyee, Z. Shao and F. Ciucci, *Chem. Rev.*, 2015, **115**, 9869.
4 A. A. Valeeva, A. A. Rempel, S. V. Rempel, S. I. Sadovnikov and A. I. Gusev, *Russ. Chem. Rev.*, 2021, **90**, 601.
5 A. A. Valeeva and A. I. Gusev, *Mendeleev Commun.*, 2022, **32**, 302.
6 N. R. Reddy, P. M. Reddy, N. Jyothi, A. S. Kumar, J. H. Jung and S. W. Joo, *J. Alloys Compd.*, 2023, **935**, 167713.
7 A. A. Valeeva, S. Z. Nazarova and A. A. Rempel, *J. Alloys Compd.*, 2020, **817**, 153215.
8 A. A. Rempel and A. A. Valeeva, *Russ. Chem. Bull.*, 2019, **68**, 2163.
9 S. Reghunath, D. Pinheiro and S. Devi KR, *Applied Surface Science Advances*, 2021, **3**, 100063.
10 D. Jiang, T. A. Otitoju, Y. Ouyang, N. F. Shoparwe, S. Wang, A. Zhang and S. Li, *Catalysts*, 2021, **11**, 1039.
11 J. Akter, M. Abu Hanif, M. A. Islam, K. P. Sapkota and J. R. Hahn, *Sci. Rep.*, 2021, **11**, 9490.
12 Y. Song, X. Lu, Z. Liu, W. Liu, L. Gai, X. Gao and H. Ma, *Nanomaterials*, 2022, **12**, 291.
13 S. Girish Kumar and K. S. R. Koteswara Rao, *Nanoscale*, 2014, **6**, 11574.
14 A. A. Haidry, Y. Wang, F. Qawareer, A. Raza, L. Zhong, H. Chen, C. R. Mandebvu and F. Ghani, *TrAC, Trends Anal. Chem.*, 2024, **170**, 117454.
15 M. Wang, W. Huang, Z. Shen, J. Gao, Y. Shi, T. Lu and Q. Shi, *J. Alloys Compd.*, 2019, **774**, 1189.
16 Z. Shen, Q. Shi, W. Huang, B. Huang, M. Wang, J. Gao, Y. Shi and T. Lu, *Appl. Phys. Lett.*, 2017, **111**, 191902.
17 K. Yoshimatsu, O. Sakata and A. Ohtomo, *Sci. Rep.*, 2017, **7**, 12544.
18 D. Wei, W. Huang, Q. Shi, T. Lu and B. Huang, *J. Mater. Sci.: Mater. Electron.*, 2016, **27**, 4216.
19 D. G. Kellerman, V. A. Zhilyaev, V. A. Perelyaev and G. P. Shveikin, *Inorg. Mater.*, 1983, **19**, 221 (*Izv. Akad. Nauk SSSR, Neorg. Mater.*, 1983, **19**, 246).
20 S. Åsbrink and A. Magnéli, *Acta Crystallogr.*, 1959, **12**, 575.
21 H. Iwasaki, N. F. H. Bright and J. F. Rowland, *J. Less-Common Met.*, 1969, **17**, 99.
22 A. A. Rusakov and G. S. Zhdanov, *Dokl. Akad. Nauk SSSR*, 1951, **77**, 411 (in Russian).
23 H.-J. Steiner, X. Turrillas and B. C. H. Steele, *J. Mater. Chem.*, 1992, **2**, 1249.
24 P. Zhao, G. Li, W. Li, P. Cheng, Z. Pang, X. Xiong, X. Zou, Q. Xu and X. Lu, *Trans. Nonferrous Met. Soc. China*, 2021, **31**, 3310.
25 W. H. Hall, *Proc. Phys. Soc., London, Sect. A*, 1949, **62**, 741.
26 G. K. Williamson and W. H. Hall, *Acta Metall.*, 1953, **1**, 22.
27 A. A. Valeeva, H. Schröttner and A. A. Rempel, *Russ. Chem. Bull.*, 2014, **63,** 2729.
28 A. A. Valeeva, A. A. Sushnikova and A. A. Rempel, *Inorg. Chem. Commun.*, 2024, **159**, 111727.
29 E. A. Kozlova, A. A. Valeeva, A. A. Sushnikova, A. V. Zhurenok and A. A. Rempel, *Nanosyst.: Phys., Chem., Math.*, 2022, **13**, 632.
30 I. Arro, V. Arro and J. Viira, *Eesti NSV Tead. Akad. Toim., Keem.*, 1987, **36**, 126 (in Russian), DOI: 10.3176/chem.1987.2.07.

Received: 7th March 2024; Com. 24/7414